Joint Input Shaping and Feedforward for Point-to-Point Motion: Automated Tuning for an Industrial Nanopositioning System

Frank Boeren,[1,*], Dennis Bruijnen[2], Niels van Dijk[2], Tom Oomen[1]

Abstract

Feedforward control can effectively compensate for the servo error induced by the reference signal if it is tuned appropriately. This paper aims to introduce a new joint input shaping and feedforward parametrization in iterative feedforward control. Such a parametrization has the potential to significantly improve the performance for systems executing a point-to-point reference trajectory. The proposed approach enables an efficient optimization procedure with global convergence. A simulation example and an experimental validation on an industrial motion system confirm i) the performance improvement obtained by means of the joint input shaping and feedforward parametrization compared to pre-existing results, and ii) the efficiency of the proposed optimization procedure.

Keywords: Feedforward Control, input shaping, precision motion systems, data-driven control

1. INTRODUCTION

Feedforward control is widely used in systems that are subject to stringent performance requirements, since feedforward can effectively compensate for the servo error induced by the reference signal. For motion systems, significant performance enhancements have been reported by using feedforward, including model-based feedforward and Iterative Learning Control (ILC), to compensate for the error signal induced by the reference trajectory, see, e.g., [1], [2], [3] and [4].

Model-based feedforward results in general in good performance and facilitates extrapolation capabilities of reference trajectories. In model-based feedforward, a parametric model is determined that approximates the inverse of the system [2], [5]. The performance improvement induced by model-based feedforward is highly dependent on i) the model quality of the parametric model of the system and ii) the accuracy of model-inversion [6]. ILC results in superior performance with respect to model-based feedforward, but in general at the expense of poor extrapolation capabilities with respect to varying reference trajectories. By learning from previous iterations, high performance is obtained for a single, specific reference trajectory.

The approach presented in [7] combines the advantages of model-based feedforward and ILC, resulting in both high performance and extrapolation capabilities of reference trajectories. To this purpose, basis functions are introduced such that the feedforward controller approximates the inverse of the system. In [8] and [9] it is shown that such an iterative feedforward approach with polynomial basis functions results in a significant performance improvement for an industrial motion system. This is explained by observing that the rigid-body dynamics and quasi-static behavior of a motion system, i.e., the dynamical behavior responsible for the dominant contribution to the servo error, are captured by polynomial basis functions [10]. In addition, in [11] it is shown that the feedforward controller is determined by means of convex optimization with an analytic solution.

Next-generation motion systems exhibit flexible dynamical behavior at lower frequencies, see, e.g., [12]. As a result, the dynamical behavior responsible for the dominant contribution to the servo error is not fully encompassed by a feedforward controller consisting of polynomial basis functions, hampering the performance of the system. The introduction of a rational basis in [13] has the potential to increase performance by improving the model quality of the feedforward controller. However, by expanding the set of admissible basis functions, the approach presented in [13] has no analytic solution.

Although iterative feedforward control with a rational basis is promising for motion systems that exhibit flexible dynamics, this parametrization i) results in an optimization problem that has no analytic solution and is in general non-convex and ii) stability of the feedforward controller is not guaranteed. In this paper it is shown that both deficiencies can be eliminated for systems executing a point-to-point motion. To this purpose, a novel connection is established between iterative feedforward control [8], [11] and input shaping [14], [15], and [16].

The main contribution of this paper is the introduction of a joint input shaping and feedforward framework for motion systems with pronounced flexible dynamical behavior that are executing a point-to-point reference trajectory. The proposed parametrization for the input shaper and feedforward i) results in an optimization problem with an analytic solution and

*Corresponding author. Tel.: +31 40 2474517. Email: f.a.j.boeren@tue.nl.
[1]Department of Mechanical Engineering, Eindhoven University of Technology, P.O. Box 513, Eindhoven 5600 MB, The Netherlands.
[2]Philips Innovation Services, High Tech Campus 7, 5656 AE Eindhoven, The Netherlands.

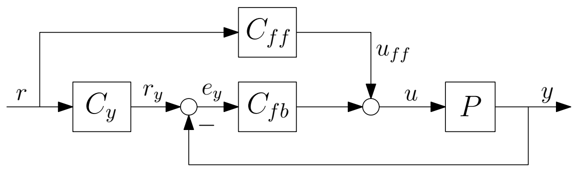

Figure 1: Two degree-of-freedom control configuration.

ii) guarantees stability of the feedforward controller and input shaper. This paper is an extended version of [17] and includes extended experimental and simulation results, and an extensive explanation and analysis.

This paper is organized as follows. In Section 2, the problem definition is stated. Then, in Section 3, a joint input shaping and feedforward framework is proposed. In Section 4, a simulation example is provided that reveals the advantages of the proposed framework compared to existing approaches. In Section 5, experimental results of the proposed approach are presented. Finally, conclusions are provided in Section 6.

2. PROBLEM DEFINITION

2.1. Joint input shaping and feedforward control goal

Consider the control configuration as depicted in Fig. 1. The true unknown system P is assumed to be discrete-time, single-input single-output, and linear time-invariant. The control configuration consists of a given stabilizing feedback controller C_{fb}, input shaper C_y, and feedforward controller C_{ff}. Furthermore, let r denote the known reference signal, r_y the filtered reference signal, u_{ff} the feedforward signal, u the input to P, y the output signal, and e_y the error signal. For the considered class of systems, a sequence of finite time tasks is executed during normal operation, where r is not necessarily the same for each consecutive task.

For a system executing a point-to-point reference trajectory, the goal of a joint input shaping and feedforward design is to obtain zero-settling behavior at the desired endposition, as shown in Fig. 2. Throughout this paper, r is designed as a 4$^{\text{th}}$ order positioning trajectory, which satisfies constraints on, e.g., actuator forces, and acceleration and velocity profiles, see, e.g., [10]. As elaborated in Sect. 3, the presented assumption enables the use of unconstrained optimization to determine C_y and C_{ff} in Fig. 1.

In this paper, performance of the joint input shaping and feedforward design is defined with respect to the known reference r. That is, high performance is obtained if $e = r - y$ is small in the dwell period $t \in [t_2,\ t_3]$. The transfer function from r to e is given by

$$e = r - y = (1 - SP(C_{ff} + C_{fb}C_y))r, \tag{1}$$

where $S = (1 + PC_{fb})^{-1}$. It is emphasized that the adopted performance definition considers the error between the known reference r and output y, and is therefore not necessarily identical to $e_y = r_y - y$. To proceed, an optimization problem is defined in the next section to iteratively update C_{ff} and C_y based on measured data.

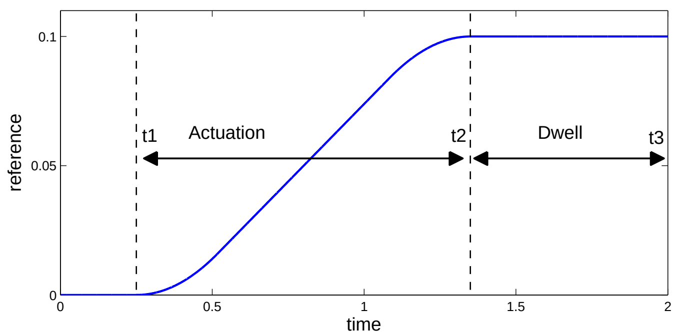

Figure 2: Point-to-point reference signal r. The goal is to obtain zero-settling behavior at the desired endposition, i.e., all vibrations in the system are compensated after completion of the motion.

2.2. Iterative input shaping and feedforward control

In iterative input shaping and feedforward control, measured data from the j^{th} task is exploited to update C_y^j and C_{ff}^j such that e is minimized. The corresponding optimization problem is given in Def. 1.

Definition 1. *Given measured signals e_y^j, u^j and y^j obtained during the j^{th} task of the closed-loop system in Fig. 1 with C_{ff}^j and C_y^j implemented. Then, the feedforward controller and input shaper in the $(j+1)^{th}$ task are given by*

$$\begin{aligned} C_{ff}^{j+1} &= C_{ff}^j + C_{ff}^\Delta, \\ C_y^{j+1} &= C_y^j + C_y^\Delta, \end{aligned} \tag{2}$$

where the update $C_{ff}^\Delta, C_y^\Delta$ based on e_y^j, u^j and y^j result from the optimization problem

$$\min_{C_{ff}^\Delta, C_y^\Delta \in \mathcal{C}} V(C_{ff}^\Delta, C_y^\Delta), \tag{3}$$

with parametrization $\mathcal{C}$ and objective function $V(C_{ff}^\Delta, C_y^\Delta)$.

The objective function $V(C_{ff}^\Delta, C_y^\Delta)$ and parametrization $\mathcal{C}$ are essential for the performance of the overall system. Typically, the objective function

$$V_2(C_{ff}^\Delta, C_y^\Delta) = \left\|\hat{e}^{j+1}(C_{ff}^\Delta, C_y^\Delta)\right\|_2^2, \tag{4}$$

is employed [8], [17], where

$$\hat{e}^{j+1} = e^j - SPC_{ff}^\Delta r - SPC_{fb}C_y^\Delta r. \tag{5}$$

To clarify (5), observe that the predicted error in the $(j+1)^{\text{th}}$ task is given by

$$\hat{e}^{j+1} = (1 - SP(C_{ff}^{j+1} + C_{fb}C_y^{j+1}))r.$$

Substitute (2) and rearrange terms to obtain

$$\hat{e}^{j+1} = (1 - SP(C_{ff}^j + C_{fb}C_y^j))r - SP(C_{ff}^\Delta + C_{fb}C_y^\Delta)r.$$

Since the first term constitutes the error e^j in the j^{th} task, this expression is equivalent to (5).

A suitable parametrization $\mathcal{C}$ is essential for the attainable performance of the system in Fig. 1. In the next section, two existing parametrizations are presented that only employ a feedforward controller C_{ff}.

Table 1: Feedforward and input shaper parametrizations for C_{pol}, C_{rat} and C_{com}, with polynomial basis functions ψ_i and parameters θ.

	C_{pol}	C_{rat}	C_{com}
C_{ff}	$\sum_{i=1}^{n_a} \psi_i\theta_i$	$\dfrac{\sum_{i=1}^{n_a} \psi_i\theta_i}{\sum_{i=n_a+1}^{n_a+n_b} \psi_i\theta_i}$	$\sum_{i=1}^{n_a} \psi_i\theta_i$
C_y	1	1	$1 + \sum_{i=n_a+1}^{n_a+n_b} \psi_i\theta_i$

2.3. Feedforward controller parametrization

In this section, C is defined for a polynomial and rational basis. These parametrizations have in common that $C_y = 1$. For this case, (1) is equal to

$$e = S(I - PC_{ff})r,$$

which reveals that e is equal to zero if $C_{ff} = P^{-1}$. Consider the polynomial parametrization C_{pol} that encompasses common parametrizations in feedforward control for motion systems, including [10], [8] and [18].

Definition 2. *The feedforward controller C_{ff} parametrized in terms of polynomial basis functions is defined as*

$$C_{pol} = \left\{ C_{ff} \mid C_{ff} = A(q^{-1}, \theta), \theta \in \mathbb{R}^{n_a} \right\},$$

where

$$A(q^{-1}, \theta) = \sum_{i=1}^{n_a} \psi_i(q^{-1})\theta_i,$$

with polynomial basis functions $\psi_i(q^{-1})$.

Similar to [10], polynomial basis functions are adopted that correspond to higher-order derivatives of r. For example, the basis function for velocity and acceleration are given by, respectively,

$$\psi_1(q^{-1}) = \frac{1 - q^{-1}}{T_s},$$
$$\psi_2(q^{-1}) = \frac{1 - 2q^{-1} + q^{-2}}{T_s^2}.$$

The designed basis functions facilitate an intuitive physical interpretation of the corresponding parameters θ. For example, θ_2, corresponding to the acceleration basis function ψ_2, represents the mass of the system.

The parametrization C_{pol} in Def. 2 has two important advantages. First, C_{ff} is linear in θ. Hence, for the quadratic objective function (4), (3) has an analytic solution [11]. Second, the polynomial basis of C_{pol} enforces stability of C_{ff}, since all poles are in the origin by definition.

However, by using polynomial basis functions, C_{pol} is only capable of describing $C_{ff} = P^{-1}$ if P has a unit numerator. This

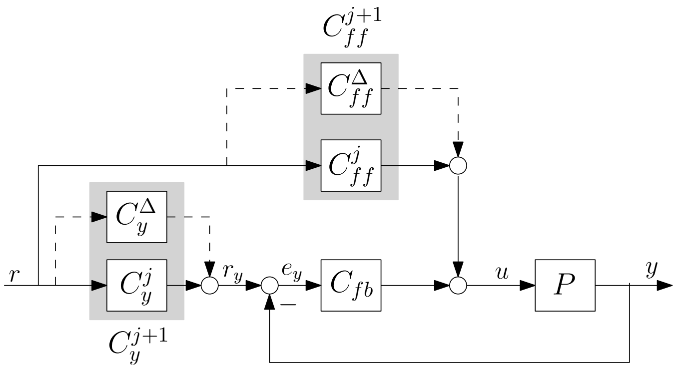

Figure 3: In the proposed joint feedforward and input shaping tuning procedure, C_{ff}^{j+1} and C_y^{j+1} are determined based on measured data from the j^{th} task by means of automated tuning.

approximation potentially leads to a significant performance deterioration. This holds in particular for motion systems with pronounced flexible dynamics, which in general violate the assumption that P has a unit numerator [19]. To enable high performance for such systems, consider the rational feedforward model structure C_{rat}, as introduced in [13, Definition 3].

Definition 3. *The feedforward controller C_{ff} parametrized in terms of a rational basis is defined as*

$$C_{rat} = \left\{ C_{ff} \mid C_{ff} = \frac{A(q^{-1}, \theta)}{B(q^{-1}, \theta)}, \theta \in \mathbb{R}^{n_a+n_b} \right\},$$

where

$$B(q^{-1}, \theta) = \sum_{i=n_a+1}^{n_a+n_b} \psi_i(q^{-1})\theta_i.$$

The parametrization C_{rat} in Def. 3 allows C_{ff} to contain both poles and zeros. This enables the design of C_{ff} such that $C_{ff} = P^{-1}$ if P is a rational model.

The key caveat associated with C_{rat} is that the optimization problem in Def. 1 becomes nonlinear in θ. As a result, (3) has in general no analytic solution. Typically, non-convex optimization is required to determine C_{ff}. In addition, stability of C_{ff} is not guaranteed, since C_{ff} contains poles at arbitrary locations. Hence, internal stability of the overall system in Fig. 1 is not guaranteed.

2.4. Problem Definition

In view of the limitations of existing parametrizations for feedforward controllers, this paper aims to investigate a joint input shaping and feedforward control framework for motion systems executing a point-to-point motion. The proposed joint input shaping and feedforward approach is defined in the following goal.

Goal 1. *Determine C_{ff} and C_y such that $V_2(C_{ff}^{\Delta}, C_y^{\Delta})$ in* (4) *is minimized during $t \in [t_2,\ t_3]$ in Fig. 2, while resorting on an optimization method which has an analytic solution.*

3. NOVEL COMBINATION OF INPUT SHAPING AND FEEDFORWARD CONTROL

In this section, a joint input shaping and feedforward framework is presented, which constitutes the main contribution of this paper. As outlined in Sect. 2.2, iterative input shaping and feedforward control is a methodology to update C_{ff} and C_y after each task. First, a parametrization for C_y and C_{ff} is presented that eliminates the deficiencies of the polynomial and rational feedforward parametrizations in Sect. 2.3 for systems executing a point-to-point motion trajectory. Second, a data-driven method is proposed to determine C_{ff} and C_y based on measured data.

3.1. Input Shaper and Feedforward Parametrization

In this section, a parameterization is proposed for C_{ff} and C_y. Consider this parametrization C_{com} given in the next definition.

Definition 4. *The feedforward controller C_{ff} and input shaper C_y parametrized in terms of polynomial basis functions are defined as*

$$C_{com} = \left\{ (C_{ff}, C_y) \middle| \begin{array}{c} C_{ff} = A(q^{-1}, \theta) \\ C_y = B(q^{-1}, \theta) \end{array}, \theta \in \mathbb{R}^{n_a+n_b} \right\},$$

where

$$A(q^{-1}, \theta) = \sum_{i=1}^{n_a} \psi_i(q^{-1})\theta_i,$$

$$B(q^{-1}, \theta) = 1 + \sum_{i=n_a+1}^{n_a+n_b} \psi_i(q^{-1})\theta_i,$$

with parameters

$$\theta = [\theta_1, \theta_2, \dots \theta_{n_a}, \theta_{n_a+1}, \theta_{n_a+2}, \dots \theta_{n_a+n_b}]^T \in \mathbb{R}^{n_a+n_b},$$

and polynomial basis functions given by

$$\Psi = [\psi_1, \psi_2, \dots, \psi_{n_a}, \psi_{n_a+1}, \psi_{n_a+2}, \dots, \psi_{n_a+n_b}]. \tag{6}$$

An overview of the parametrizations C_{com}, C_{pol} and C_{rat} is provided in Table 1. The following constraint is imposed on the input shaper

$$C_y(q^{-1}, \theta)|_{q^{-1}=1} = 1. \tag{7}$$

This constraint enforces unit d.c. gain to avoid scaling of the reference r. In addition, by observing that $r_y = C_y r$ it follows that $r_y = r$ in $t \in [t_2 + N, \; t_3]$, where $N = n_b - n_a$ is the order of C_y, as illustrated in Fig. 4. This observation is a crucial attribute of the optimization procedure presented in the next section.

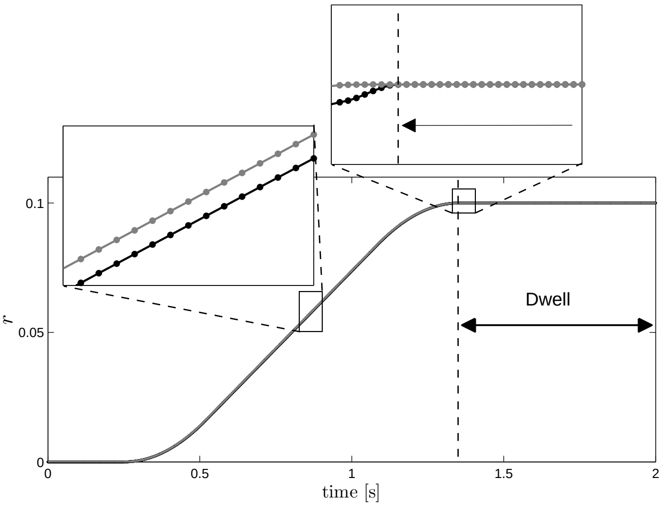

Figure 4: The shaped reference r_y (black) is delayed with respect to the reference r (grey) since $r_y = C_y(q^{-1}, \theta)r$. However, the constraint $C_y(q^{-1}, \theta)|_{q^{-1}=1} = 1$ implies that $r_y = r$ in the dwell period $[t_2 + N, t_3]$.

3.2. Approach to iterative feedforward and input shaping

As stated in Goal 1, high performance is obtained if the objective function $V_2(C_{ff}^{\Delta}, C_y^{\Delta})$ in (4) is minimal in $t \in [t_2, \; t_3]$. For the problem setting in this paper, an indirect approach is pursued to achieve this goal. That is, for the optimization problem (3) as stated in Def. 1, the parametrization is given by C_{com} in Def. 4, while the objective function yields

$$V_y(C_{ff}^{\Delta}, C_y^{\Delta}) = \left\| \hat{e}_y^{j+1}(C_{ff}^{\Delta}, C_y^{\Delta}) \right\|_2^2,$$

with predicted error $\hat{e}_y^{j+1}$ in the $(j+1)^{\text{th}}$ iteration given by

$$\hat{e}_y^{j+1} = e_y^j + S(C_y^{\Delta} - PC_{ff}^{\Delta})r. \tag{8}$$

The motivation for the pursued indirect approach is twofold. First, this approach exploits measured data from $t \in [t_1, \; t_3]$ to determine the parameters θ of C_y and C_{ff}, which is clearly beneficial for convergence of θ. Second, by observing that the transfer from r to e_y in Fig. 1 is given by

$$e_y = S(C_y - PC_{ff})r,$$

it becomes clear that e_y is equal to zero if $C_{ff}C_y^{-1} = P^{-1}$. This implies that the reference-induced contribution to e_y is eliminated if the numerator and denominator of P are described by C_y and C_{ff}, respectively. This interpretation of the optimal C_y and C_{ff} is in accordance with the expressions derived in Sect. 2.3 for the polynomial and rational feedforward parametrization.

It remains to be shown that the pursued optimization with $V_y(C_{ff}^{\Delta}, C_y^{\Delta})$ instead of $V_2(C_{ff}^{\Delta}, C_y^{\Delta})$ indeed attains Goal 1. To illustrate the validity of the pursued approach, observe that the constraint (7) as imposed on the input shaper in Sect. 3.1, implies that $V_2(C_{ff}^{\Delta}, C_y^{\Delta}) = V_y(C_{ff}^{\Delta}, C_y^{\Delta})$ during $t \in [t_2 + N, \; t_3]$, as depicted in Fig. 2. To illustrate this statement, observe that $\hat{e}^{j+1}$ in (5) is equal to

$$\hat{e}^{j+1} = (1 - SP(C_{ff}^{j+1} + C_{fb}C_y^{j+1}))r, \tag{9}$$

and $\hat{e}_y^{j+1}$ in (8) is equivalent to

$$\hat{e}_y^{j+1} = S(C_y^{j+1} - PC_{ff}^{j+1})r. \tag{10}$$

As presented in Fig. 4, (7) implies that $C_y^{j+1}r$ is equal to r in $t \in [t_2 + N,\ \ t_3]$. Substitute this result in (9) and (10), rearrange terms and evaluate for $t \in [t_2 + N,\ \ t_3]$ to obtain

$$\hat{e}^{j+1} = (1 - T)r - SPC_{ff}^{j+1}r,$$

with complementary sensitivity $T = PC_{fb}S$, and

$$\hat{e}_y^{j+1} = S(1 - PC_{ff}^{j+1})r.$$

Since $1 - T = S$, it readily follows that $\hat{e}^{j+1}$ and $\hat{e}_y^{j+1}$ are equivalent in $t \in [t_2 + N,\ \ t_3]$. As a result, $V_2(C_{ff}^{\Delta}, C_y^{\Delta}) = V_y(C_{ff}^{\Delta}, C_y^{\Delta})$ in this time interval, motivating the proposed indirect approach based on the optimization problem (3) with C_{com} and $V_y(C_{ff}^{\Delta}, C_y^{\Delta})$.

The disadvantage of the pursued indirect approach is the discrepancy between V_y and V_2 in $t \in [t_2,\ \ t_2 + N]$. This discrepancy potentially hampers the achievable performance during the dwell period if N, the order of the polynomial C_y, is large compared to the settling time of the system. However, for motion systems with flexible dynamics, a limited number of parameters is typically sufficient to compensate for the dominant component of the reference-induced error. That is, $C_{ff}C_y^{-1}$ should only accurately represent P^{-1} in frequency ranges where r has significant power content. For an 4^{th} point-to-point reference trajectory, this is typically the low-frequency range [10], [19]. As a result, the order N of C_y is limited, even for a system P with multiple vibration modes, and the performance improvement in $t \in [t_2,\ \ t_3]$ due to C_y significantly dominates the performance loss in $t \in [t_2,\ \ t_2 + N]$.

3.3. Optimization Algorithm

In this section, the optimization problem in Def. 1 with C_{com} and $V_y(C_{ff}^{\Delta}, C_y^{\Delta})$ is reformulated as a linear least squares problem. It is shown that the parametrization C_{com} proposed in Def. 4 is crucial to obtain an analytic expression for θ.

The following results are required in a data-driven method to determine C_{ff}^{Δ} and C_y^{ff} in (3), i.e., without explicitly constructing parametric or nonparametric models of closed-loop transfer functions. Define $C = (C_{fb}C_y^j + C_{ff}^j)$. Consider the transfer function from r to y^j in the j^{th} task for the closed-loop system in Fig. 3 given by

$$y^j = SP(C_{fb}C_y^j + C_{ff}^j)r. \tag{11}$$

Since all transfer function are SISO, (11) is equivalent to

$$SPr = (C_{fb}C_y^j + C_{ff}^j)^{-1}y^j = C^{-1}y^j. \tag{12}$$

In addition, the transfer function from r to u in the j^{th} task

$$u^j = S(C_{fb}C_y^j + C_{ff}^j)r,$$

is reformulated as

$$Sr = (C_{fb}C_y^j + C_{ff}^j)^{-1}u^j = C^{-1}u^j. \tag{13}$$

A proof follows along the same lines as in [8]. Expressions (12) and (13) enable the estimation of θ in Def. 4 solely based on measured data, as proposed in the following theorem.

Theorem 1. *Given measured signals e_y, u^j and y^j. Then, for $(C_{ff}, C_y) \in C_{com}$, minimization of* (3) *with respect to θ^{Δ}*

$$\hat{\theta}^{\Delta} = \arg\min_{\theta^{\Delta}} V_y(C_{ff}^{\Delta}, C_y^{\Delta}), \tag{14}$$

is equivalent to the least squares solution to

$$\Phi\hat{\theta}^{\Delta} = e_y^j, \tag{15}$$

with

$$\Phi = \Psi C^{-1}\begin{bmatrix} y^j \\ u^j \end{bmatrix} \in \mathbb{R}^{N\times(n_a+n_b)}.$$

Proof. Exploiting the commutative property of SISO systems in (8) results in

$$\hat{e}_y^{j+1}(\theta^{\Delta}) = e_y^j + SrC_y^{\Delta} - SPrC_{ff}^{\Delta}, \tag{16}$$

Substitution of (12) and (13) in (16) yields

$$\begin{aligned}\hat{e}_y^{j+1}(\theta^{\Delta}) &= e_y^j + C_y^{\Delta}C^{-1}u^j - C_{ff}^{\Delta}C^{-1}y^j,\\ &= e_y^j - \Phi\theta^{\Delta}.\end{aligned}$$

Since C_{ff}^{Δ} and C_y^{Δ} are linear in θ^{Δ} and $V_y(C_{ff}^{\Delta}, C_y^{\Delta})$ is a positive-definite function, $\hat{\theta}^{\Delta}$ is the unique solution to

$$\frac{\partial V_y(C_{ff}^{\Delta}, C_y^{\Delta})}{\partial\theta^{\Delta}}\Big|_{\theta^{\Delta}=\hat{\theta}^{\Delta}} = 0,$$

resulting in the linear least squares problem formulated in (15). □

Remark 1. *In [17, Section 2.D], nonlinear optimization is used to solve* (14)*. Inspired by iterative feedback tuning (IFT) [20], this procedure to determine C_{ff}^{Δ} and C_y^{Δ} relies on approximations of the Hessian and gradient of $V_y(C_{ff}^{\Delta}, C_y^{\Delta})$, resulting in an estimate of θ^{Δ}. However, Thm. 1 shows that the optimization problem with respect to θ^{Δ} has an analytic solution.*

The least squares solution to (15) is equivalent to

$$\hat{\theta}^{\Delta} = (\Phi^T\Phi)^{-1}\Phi^T e_y^j.$$

The following assumption ensures that $\hat{\theta}^{\Delta}$ can be uniquely determined.

Assumption 1. $\Phi^T\Phi$ *is nonsingular.*

Assumption 1 imposes a persistence of excitation condition on r.

Remark 2. *Preview-based stable inversion [21] can be directly employed to compute $C^{-1}y^j$ and $C^{-1}u^j$ if C^{-1} is unstable.*

Based on $\hat{\theta}^\Delta$ obtained by means of Thm. 1, C_{ff}^{j+1} and C_y^{j+1} in Def. 1 result from the following theorem.

Theorem 2. *For $(C_{ff}^j, C_y^j), (C_{ff}^\Delta, C_y^\Delta) \in \mathcal{C}_{com}$ with identical basis functions Ψ in (6), C_{ff}^{j+1} and C_y^{j+1} in (2) are given by*

$$C_{ff}^{j+1} = \sum_{i=1}^{n_a} \psi_i \theta_i^{j+1},$$

$$C_y^{j+1} = 1 + \sum_{i=n_a+1}^{n_a+n_b} \psi_i \theta_i^{j+1},$$

where $\theta_i^{j+1} = \theta_i^j + \theta_i^\Delta$.

Proof. Since $(C_{ff}^j, C_y^j), (C_{ff}^\Delta, C_y^\Delta) \in \mathcal{C}_{\text{com}}$ have identical Ψ, C_{ff}^{j+1} and C_y^{j+1} are given by

$$C_{ff}^{j+1} = C_{ff}^j + C_{ff}^\Delta = \sum_{i=1}^{n_a} \psi_i \theta_i^j + \sum_{i=1}^{n_a} \psi_i \theta_i^\Delta,$$

$$C_y^{j+1} = C_y^j + C_y^\Delta = 1 + \sum_{i=n_a+1}^{n_a+n_b} \psi_i \theta_i^j + \sum_{i=n_a+1}^{n_a+n_b} \psi_i \theta_i^\Delta.$$

Since (C_{ff}^j, C_y^j) and $(C_{ff}^\Delta, C_y^\Delta)$ are linear in respectively θ^j and θ^Δ, superposition implies that

$$C_{ff}^{j+1} = \sum_{i=1}^{n_a} \psi_i \left(\theta_i^j + \theta_i^\Delta\right) = \sum_{i=1}^{n_a} \psi_i \theta_i^{j+1},$$

$$C_y^{j+1} = 1 + \sum_{i=n_a+1}^{n_a+n_b} \psi_i \left(\theta_i^j + \theta_i^\Delta\right) = 1 + \sum_{i=n_a+1}^{n_a+n_b} \psi_i \theta_i^{j+1}.$$

□

In this section, unconstrained optimization is employed to determine C_{ff}^{j+1} and C_y^{j+1}. This optimization method is selected to facilitate implementation of the approach in practice, since it requires small computational requirements. However, the absence of constraints on, e.g., actuator forces, acceleration and velocity forces, during optimization implies that erratic behavior of r_y and u_{ff} can occur if C_{ff}^{j+1} and C_y^{j+1} are applied to the system.

A heuristic approach is used to verify that C_{ff}^{j+1} and C_y^{j+1} can be safely applied to the system in the next task. As presented in Sect. 2.3, the basis functions ψ used in C_{ff} and C_y correspond to higher-order derivatives of r. As a result, the corresponding parameters θ have a physical interpretation. This facilitates the construction of an upper and lower bound for θ^{j+1} based on, e.g., physical insight or simulation results of the system. If the parameters θ^{j+1} are within these bounds, C_{ff}^{j+1} and C_y^{j+1} are applied to the system. Otherwise, θ^j is not updated after the j^{th} task.

Finally, consider the following procedure to determine $(C_{ff}^{j+1}, C_y^{j+1}) \in \mathcal{C}_{\text{com}}$ based on e_y^j, u^j and y^j in the j^{th} iteration, which implements the results presented in this section.

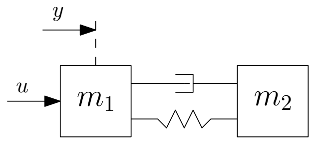

Figure 5: Schematic illustration of a two-mass spring damper setup.

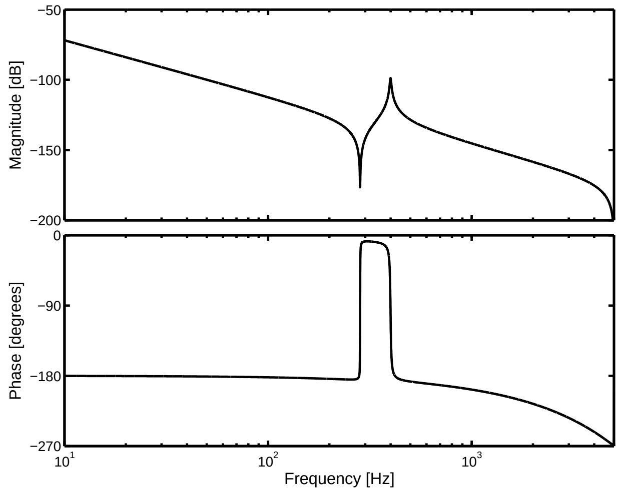

Figure 6: Bode diagram of a two-mass spring damper setup.

Procedure 1. *Estimation of $\hat{\theta}^\Delta$ in the j^{th} iteration*

1) *Measure e_y^j, u^j and y^j.*
2) *construct $\Phi = \Psi C^{-1} \begin{bmatrix} y^j & u^j \end{bmatrix}^T \in \mathbb{R}^{N \times (n_a+n_b)}$.*
3) *solve $\hat{\theta}^\Delta = (\Phi^T \Phi)^{-1} \Phi^T e_y^j$.*
4) *Construct*
$$C_{ff}^{j+1} = \sum_{i=1}^{n_a} \psi_i \left(\theta_i^j + \hat{\theta}_i^\Delta\right), \quad C_y^{j+1} = 1 + \sum_{i=n_a+1}^{n_a+n_b} \psi_i \left(\theta_i^j + \hat{\theta}_i^\Delta\right).$$
5) *Verify if C_{ff}^{j+1} and C_y^{j+1} satisfy the constraints.*

To summarize, in this section a novel joint input shaping and feedforward control framework is developed for systems executing a point-to-point motion. It is emphasized that the approach in [8] based on polynomial basis functions ($\mathcal{C}_{\text{pol}}$) is immediately recovered as a special case of the developed framework for $C_y = 1$. That is, the proposed model structure is a generalization of $\mathcal{C}_{\text{pol}}$, thereby eliminating the requirement that P has a unit numerator. Compared to a rational feedforward model structure $\mathcal{C}_{\text{rat}}$, the framework presented in this paper i) has an analytic solution and ii) internal stability of the overall system is guaranteed. These two advantages are a result of the polynomial basis for both C_y and C_{ff}, as proposed in Def. 4.

4. SIMULATION EXAMPLE

In this section, a simulation example is provided to illustrate the joint input shaping and feedforward approach $\mathcal{C}_{\text{com}}$ presented in Sect. 3. It is shown that a significant performance enhancement is obtained with respect to $\mathcal{C}_{\text{pol}}$ in Sect. 2.3 for systems with pronounced flexible dynamics.

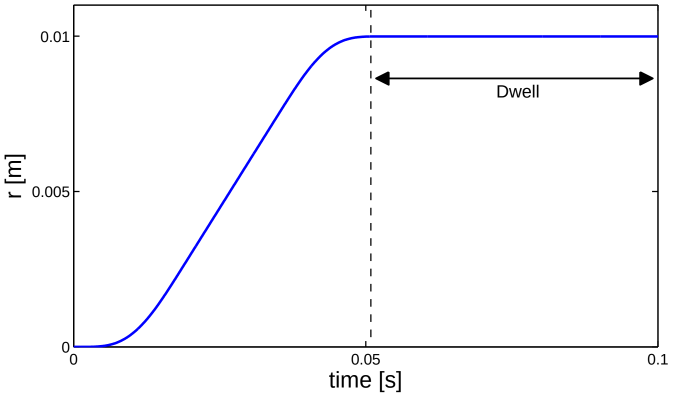

Figure 7: Reference signal applied to the closed loop system with (P, C_{fb}). The goal of the joint input shaping and feedforward design is to minimize e during the dwell period.

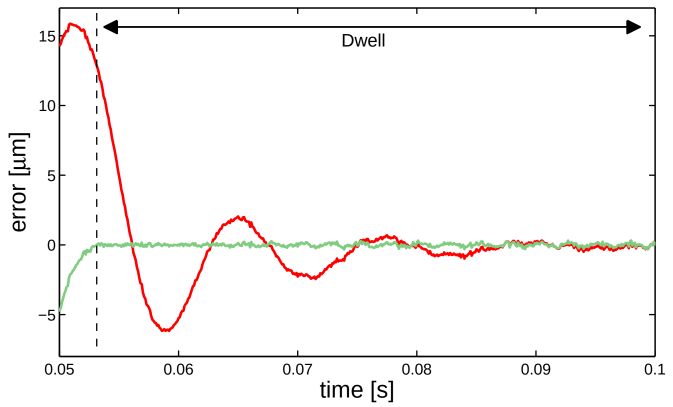

Figure 8: The error e during the dwell period visually confirms that the settling time for C_{com} (green) is significantly smaller than for C_{pol} (red).

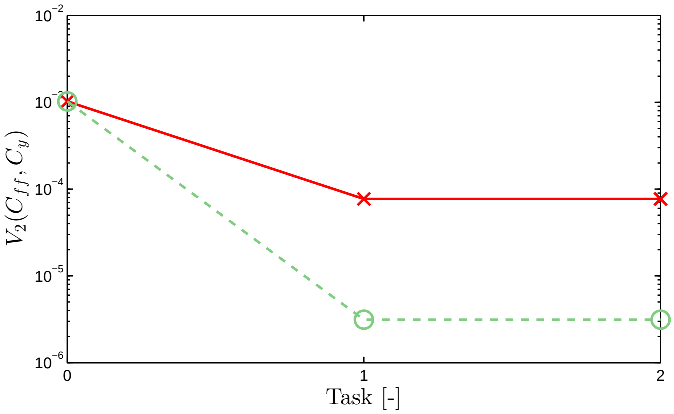

Figure 9: The objective function $V_2(C_{ff}, C_y)$ corresponding to C_{com} (dashed green) is significantly smaller than for C_{pol} (red). This confirms that the proposed approach results in performance enhancement.

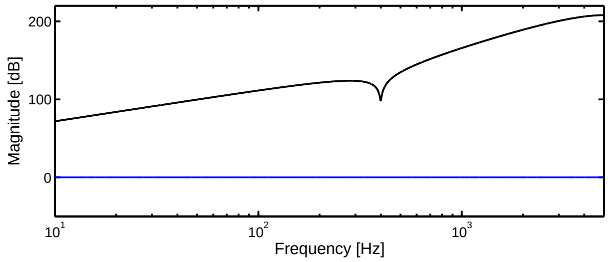

(a) C_{ff} (black) and C_y (blue).

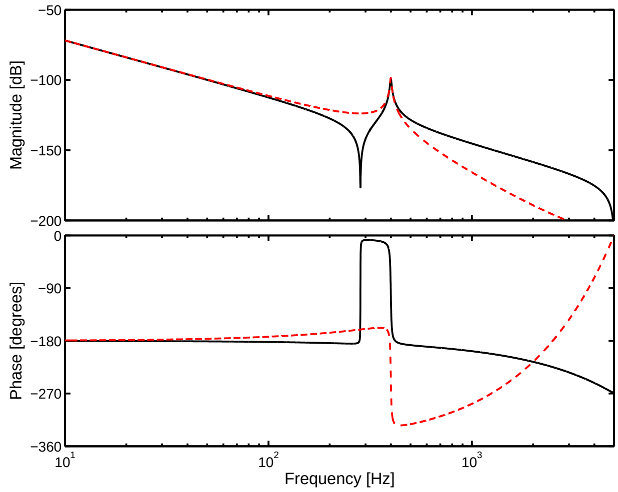

(b) P (black) and $C_y C_{ff}^{-1}$ (red dashed).

Figure 10: $C_{ff} \in C_{\text{pol}}$ - The system P is not exactly described by C_{ff}^{-1}, hampering performance of the system during the dwell period.

Consider a two-mass spring damper system as schematically depicted in Fig. 5. The dynamical behavior of this system consist of rigid body and flexible dynamics, see Fig. 6. The corresponding discrete-time transfer function is given by

$$P(z) = 9.97 \times 10^{-9} \frac{(z+1)(z^2 - 1.968z + 0.9996)}{(z-1)^2(z^2 - 1.934z + 0.9966)}. \quad (17)$$

The sampling time is equal to $T_s = 1 \times 10^{-4}$ [s]. Furthermore, the feedback controller, designed by means of manual loop-shaping, is given by

$$C_{fb}(z) = 1 \times 10^5 \frac{(z-0.99)(z-0.9833)(z^2 - 1.924z + 0.987)}{(z-1)(z-0.86)^2(z^2 - 1.823z + 0.8819)},$$

and results in a bandwidth of 80 Hz, defined as the frequency where $PC_{fb} = 1$. An output disturbance v modeled as $v = H\epsilon$ is added to the closed-loop system, where

$$H(z) = 0.7656 \frac{(z-1)^2}{(z^2 - 1.475z + 0.5869)},$$

and ϵ is zero mean white noise with standard deviation 1×10^{-7}. The system is excited by a 4rd order point-to-point reference r, as depicted in Fig. 7.

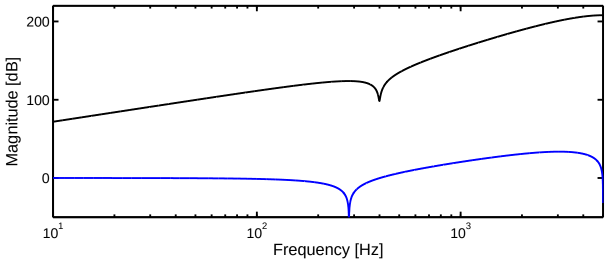

(a) C_{ff} (black) and C_y (blue).

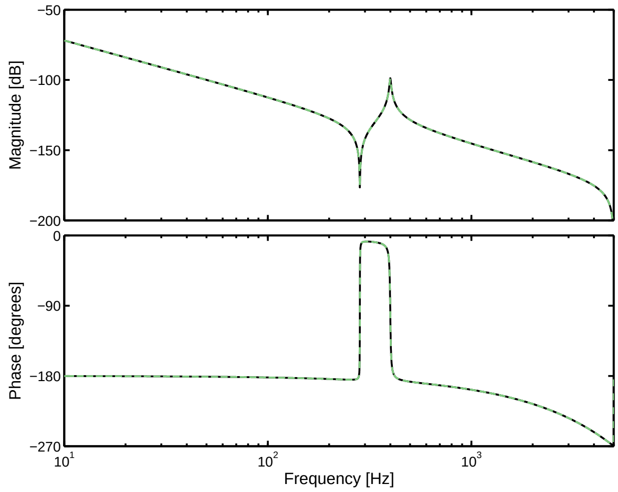

(b) P (black) and $C_y C_{ff}^{-1}$ (green dashed).

Figure 11: $(C_y, C_{ff}) \in \mathcal{C}_{\mathrm{com}}$: P is exactly described by $C_y C_{ff}^{-1}$, resulting in superior performance in dwell period.

The input shaper C_y and feedforward controller C_{ff} are parametrized as 4th order filters given by

$$C_y(q^{-1}, \theta) = 1 + \psi_1\theta_1 + \psi_2\theta_2 + \psi_3\theta_3 + \psi_4\theta_4,$$
$$C_{ff}(q^{-1}, \theta) = \psi_5\theta_5 + \psi_6\theta_6 + \psi_7\theta_7,$$

with basis functions

$$\psi_1(q^{-1}) = \frac{1 - q^{-1}}{T_s},$$
$$\psi_2(q^{-1}) = \psi_5(q^{-1}) = \frac{1 - 2q^{-1} + q^{-2}}{T_s^2},$$
$$\psi_3(q^{-1}) = \psi_6(q^{-1}) = \frac{1 - 3q^{-1} + 3q^{-2} - q^{-3}}{T_s^3},$$
$$\psi_4(q^{-1}) = \psi_7(q^{-1}) = \frac{1 - 4q^{-1} + 6q^{-2} - 4q^{-3} + q^{-4}}{T_s^4}.$$

The initial values of the parameters θ yield

$$\theta^{\mathrm{init}} = \left[0,\ 0,\ 0,\ 0,\ 9 \times 10^{-1},\ 0,\ 0\right]^T,$$

i.e., only the acceleration term in C_{ff} is initialized.

The error e during the dwell period as depicted in Fig. 8 illustrates that the settling time for $(C_y, C_{ff}) \in \mathcal{C}_{\mathrm{com}}$ is significantly smaller than for $C_{ff} \in \mathcal{C}_{\mathrm{pol}}$. This is confirmed by the objective function $V_2(C_{ff}, C_y)$ as depicted in Fig. 9, which shows that the two-norm of e in the dwell period is significantly smaller for $\mathcal{C}_{\mathrm{com}}$ than for $\mathcal{C}_{\mathrm{pol}}$. Hence, the simulation results confirm

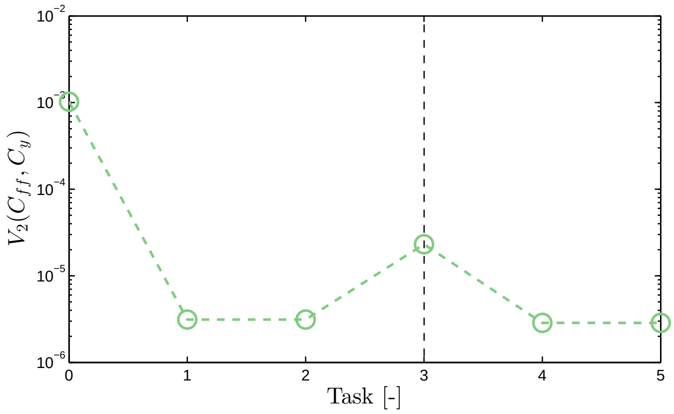

Figure 12: The objective function $V_2(C_{ff}, C_y)$ for $\mathcal{C}_{\mathrm{com}}$ (dashed green), where the dynamical behavior of P changes after the second task. As a result, performance deteriorates in the third task. By exploiting measured data from the third task, C_{ff} and C_y are updated to obtain superior performance in the fourth and fifth task.

that the performance of the system is significantly enhanced by means of the model structure $\mathcal{C}_{\mathrm{com}}$ compared to $\mathcal{C}_{\mathrm{pol}}$.

Consider the visualization of $\mathcal{C}_{\mathrm{pol}}$ and $\mathcal{C}_{\mathrm{com}}$ in Fig. 10 and Fig. 11, respectively. On the one hand, as depicted in Fig. 10, a feedforward parametrization $\mathcal{C}_{\mathrm{pol}}$ is only capable of capturing the dynamical behavior of P in the frequency range up to approximately 80 Hz. This implies that it is not possible to compensate for the excitation of flexible dynamics by the setpoint through this parametrization of C_y and C_{ff}. This is explained by observing that $C_y C_{ff}^{-1}$ for $\mathcal{C}_{\mathrm{pol}}$ is only capable of describing a system P with a unit numerator.

On the other hand, the proposed joint input shaping and feedforward approach is capable of describing the dynamical behavior of flexible dynamics, as depicted in Fig. 11. This clearly illustrates the advantages of the proposed approach with respect to conventional approaches for a system P described by a rational model, such as motion systems exhibiting flexible dynamics. It is emphasized that for $C_{ff} \in \mathcal{C}_{\mathrm{rat}}$, a similar performance can be obtained as with $\mathcal{C}_{\mathrm{com}}$. However, the proposed approach has significant advantages for systems executing a point-to-point motion reference, as presented in Sect. 3.

Finally, it is shown that variations in the dynamical behavior of P can be effectively compensated by means of the proposed iterative procedure. To this purpose, assume that between the second and third task, $P(z)$ as given in (17) is replaced by the perturbed system

$$P_\Delta(z) = 9.97 \times 10^{-9} \frac{(z+1)(z^2 - 1.968z + 0.9978)}{(z-1)^2(z^2 - 1.934z + 0.9917)}.$$

The objective function $V_2(C_{ff}, C_y)$ as depicted in Fig. 12 shows a significant performance deterioration in the third task. This is explained by observing that $C_y C_{ff}^{-1}$ in the third task is not equal to P_Δ. By exploiting measured data from the third task, C_y and C_{ff} in the fourth task are adapted such that $C_y C_{ff}^{-1} = P_\Delta$ in the fourth task. Hence, variations in the dynamics of P can be effectively compensated by means of iteratively updating C_y and C_{ff} based on measured data.

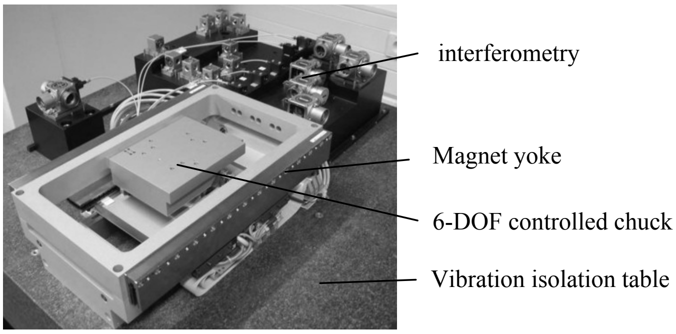

Figure 13: Experimental setup.

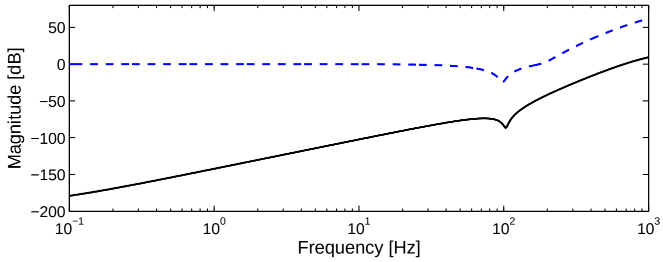

(a) C_{ff} (black) and C_y (blue).

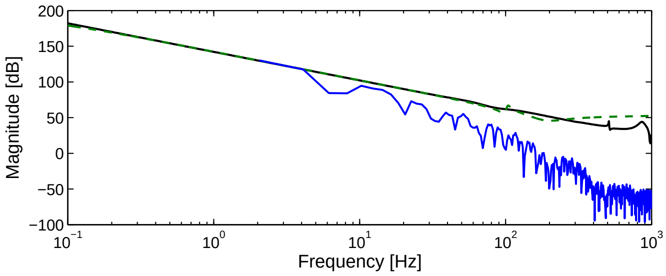

(b) P (black), $C_yC_{ff}^{-1}$ (green dashed) and power spectral density of r.

Figure 14: The system P is accurately described by $C_yC_{ff}^{-1}$ in $f \in [0, 120]$ Hz. As confirmed by the power spectral density (PSD) of r, this is the frequency range with the dominant contribution to the reference-induced error.

5. EXPERIMENTAL RESULTS OF PROPOSED APPROACH

5.1. Experimental Setup

In this section, the combined input shaping and feedforward control approach proposed in this paper is confronted with a prototype industrial motion system. The experimental setup in Fig. 13 is controlled in all six motion degrees of freedom (DOF) (i.e., three rotations and three translations). To this purpose, the system is equipped with six actuators to provide the required force. The actuators consist of linear motors with an added position offset such that an actuator can also generate a force in the perpendicular direction. Gravity compensation magnets have been added to reduce the required static force. Laser interferometers enable nanometer resolution position measurements in the six motion degrees of freedom. A feedback controller $C_{fb}(z)$ is determined by means of sequential loopshaping. All experiments are performed with a sampling time $T_s = 2 \times 10^{-4}$ [s].

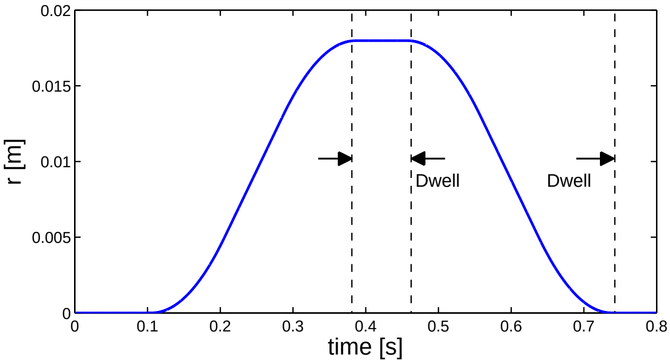

Figure 15: Point-to-point reference r with a stroke of 18 [mm] and acceleration of 1 [m/s^2].

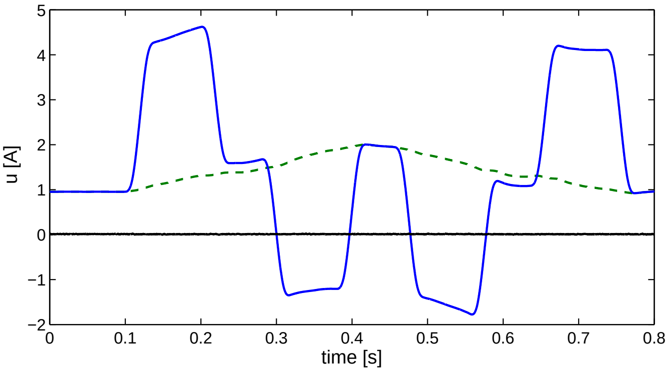

Figure 16: The contribution to u of u_{fb} (black), u_{ff} (blue) and the offset (dashed green) indicates that the feedforward contribution, consisting of the output of $C_{ff}(z, \theta)$ and the position dependent static offset, is significantly larger than the contribution of the feedback controller.

5.2. Experimental Results

Even though the experimental setup is inherently multivariable, the proposed approach is only applied to the long stroke direction x. For the feedback controller, a sequential design is pursued for this system. To this purpose, an equivalent system P_{eq} is determined for the x-direction after closing the control loops for the remaining 5 DOFs. This equivalent system P_{eq} is given by

$$P_{eq}(z) = P_{xx} - P_{xy}C_{yy}(I + P_{yy}C_{yy})^{-1}P_{yx},$$

as seen by the controller C_{xx}, and is depicted in Fig. 14. The controller C_{xx} is designed by means of manual loop-shaping and attains a bandwidth of 120 Hz.

The 4$^{\text{th}}$ order reference trajectory r depicted in Fig. 15 is used to determine C_{ff} and C_y by means of Proc. 1. As shown in Fig. 16, a position dependent static offset is applied to the system. This offset is used to compensate for nonlinear and time-varying system behavior, in order to obtain a linear time-invariant system P for feedforward optimization. The estimated 4$^{\text{th}}$ order C_{ff} and 4$^{\text{th}}$ order C_y as depicted in Fig. 14a accurately describe P in $f \in [0, 120]$ Hz, as depicted in Fig. 14b. For higher frequencies, r is not sufficiently exciting to accurately represent the system in this frequency range.

In Fig. 16, the plant input is shown. The feedback controller contribution (u_{fb}) is approximately zero compared to the feed-

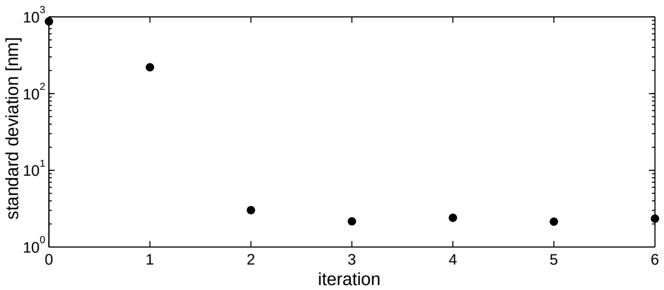

Figure 17: Optimal performance with a 4th order C_{ff} and 4th order C_y is obtained after executing two iterations on the experimental setup.

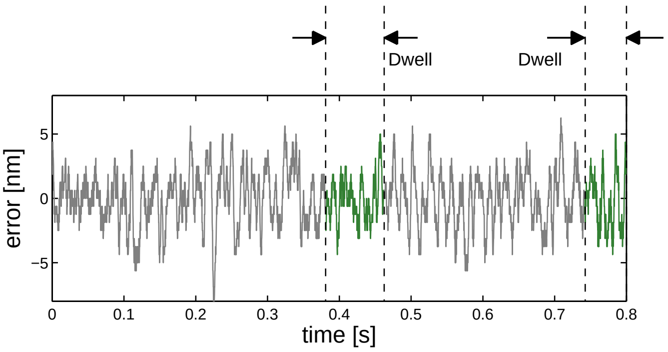

Figure 18: The standard deviation σ of the error e_y corresponding to the estimated $(C_{ff}, C_y) \in \mathcal{C}_{\text{com}}$ is equal to $\sigma = 2.3$ [nm] during the two dwell periods.

forward part (u_{ff}). This shows that the feedforward effectively compensates for the reference-induced error. In Fig. 17, it is shown that the optimal parameters θ for the 4th order C_{ff} and C_y are obtained based on measured data from two tasks. This illustrates that the presented optimization experiment is efficient.

Comparing Fig. 18 and Fig. 19 shows that the error e_y in the dwell period, obtained by means of the proposed combined input shaping and feedforward control methodology approaches the stand-still error depicted in Fig. 19. This illustrates that the proposed approach effectively compensates for the reference-induced error e after completion of a point-to-point motion. Indeed, a comparison between $\mathcal{C}_{\text{com}}$, $\mathcal{C}_{\text{pol}}$ and the case without feedforward and input shaping as provided in Table 2 confirms the benefits of the proposed approach for the considered experimental setup.

6. CONCLUSIONS

In this paper, a new approach for joint input shaping and feedforward control is presented and verified i) in a simulation study and ii) by means of an experimental confrontation with a prototype industrial motion system. The proposed model structure is a generalization of a polynomial model structure, thereby removing the restrictive condition that P has a unit numerator. It is shown that the proposed joint input shaping and feedforward model structure results in a significant performance improvement compared to pre-existing approaches for systems executing a point-to-point motion. Compared to a rational feedforward model structure, the model structure presented in this paper has two key advantages: i) there exist an analytic solution and ii) internal stability of the overall system is guaranteed.

In [11] a refinement is presented for iterative feedforward control algorithms that results in significantly enhanced accuracy and efficiency for feedforward controllers with polynomial basis functions. Future research focuses on an extension of the results in [11] and [22] to the iterative procedure proposed in this paper, multivariable generalizations, inferential control [23] and systems with position-dependent dynamics [24]. Furthermore, a thorough analysis of intersample behavior as in [25] is advised.

Table 2: Standard deviation σ in the dwell period after convergence of the optimization procedure for $\mathcal{C}_{\text{com}}$, $\mathcal{C}_{\text{pol}}$ and without feedforward and input shaping shows that the parametrization $\mathcal{C}_{\text{com}}$ results in superior performance.

	$\mathcal{C}_{\text{com}}$	$\mathcal{C}_{\text{pol}}$	C_{fb}
σ [nm]	2.3	3.6	37

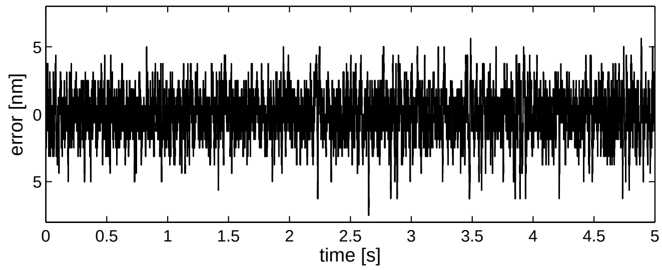

Figure 19: The error signal during stand-still is equal to $\sigma = 1.7$ [nm].

References

[1] Clayton GM, Tien S, Leang KK, Zou Q, Devasia S. A review of feedforward control approaches in nanopositioning for high-speed SPM. Journal of Dynamic Systems, Measurement, and Control 2009;131(6):0611011 – 061101–19.

[2] Butterworth J, Pao L, Abramovitch D. Analysis and comparison of three discrete-time feedforward model-inverse control techniques for nonminimum-phase systems. Mechatronics 2012;22:577–87.

[3] Rigney BP, Pao LY, Lawrence DA. Nonminimum phase dynamic inversion for settle time applications. IEEE Trans Control Systems Technology 2009;17(5):989–1005.

[4] Bristow D, Tharayil M, Alleyne A. A survey of iterative learning control. IEEE Control Systems Magazine 2006;26(3):96–114.

[5] Zhong H, Pao LY, de Callafon RA. Feedforward control for disturbance rejection: Model matching and other methods. In: Proceedings of the Chinese Conference on Decision and Control, Taiyuan, China. 2012, p. 3525–33.

[6] Devasia S. Should model-based inverse inputs be used as feedforward under plant uncertainty? IEEE Transactions on Automatic Control 2002;47(11):1865–71.

[7] van de Wijdeven J, Bosgra O. Using basis functions in iterative learning control: analysis and design theory. International Journal of Control 2010;83(4):661–75.

[8] van der Meulen S, Tousain R, Bosgra O. Fixed structure feedforward controller design exploiting iterative trials: Application to a wafer stage and a desktop printer. Journal of Dynamic Systems, Measurement, and Control 2008;130(5):0510061–05100616.

[9] Stearns H, Yu S, Fine B, Mishra S, Tomizuka M. A comparative study of feedforward tuning methods for wafer scanning systems. In: ASME Dynamic Systems and Control Conference, Michigan, USA. 2008,.

[10] Lambrechts P, Boerlage M, Steinbuch M. Trajectory planning and feedforward design for electromechanical motion systems. Control Engineering Practice 2005;13:145–57.
[11] Boeren F, Oomen T. Iterative feedforward control: a closed-loop identification problem and a solution. In: Proceedings of the 52st Conference on Decision and Control, Firenze, Italy. 2013, p. 6694–9.
[12] Oomen T, van Herpen R, Quist S, van de Wal M, Bosgra O, Steinbuch M. Connecting system identification and robust control for next-generation motion control of a wafer stage. IEEE Transactions on Control Systems Technology 2014;22(1):102–18.
[13] Bolder J, Oomen T, Steinbuch M. Exploiting rational basis functions in iterative learning control. In: Proceedings of the 52st IEEE Conference on Decision and Control, Firenze, Italy. 2013,.
[14] Singhose W. Command shaping for flexible systems: A review of the first 50 years. International Journal of Precision Engineering and Manufacturing 2009;10(4):158–68.
[15] Boettcher U, Fetzer D, Li H, de Callafon RA, Talke FE. Reference signal shaping for closed-loop systems with application to seeking in hard disk drives. IEEE Transactions on Control Systems Technology 2012;20(2):335–45.
[16] Cutforth CF, Pao LY. Adaptive input shaping for maneuvering flexible structures. Automatica 2004;40(4):685–93.
[17] Bruijnen D, van Dijk N. Combined input shaping and feedforward control for flexible motion systems. In: Proceedings of the 2012 American Control Conference, Montréal, Canada. 2012,.
[18] Heertjes M, Hennekens D, Steinbuch M. MIMO feed-forward design in wafer scanners using a gradient approximation-based algorithm. Control Engineering Practice 2010;18(5):495–506.
[19] Gawronski W. Advanced Structural Dynamics and Active Control of Structures. Springer, New York, New York, United States; 2004.
[20] Hjalmarsson H. Iterative feedback tuning - an overview. International Journal of Adaptive Control and Signal Processing 2002;16(5):373–95.
[21] Zou Q. Optimal preview-based stable-inversion for output tracking of nonminimum-phase linear systems. Automatica 2009;45(1):230–7.
[22] Boeren F, Oomen T, Steinbuch M. Accuracy aspects in motion feedforward tuning. In: Proceedings of the American Control Conference, Portland, OR, USA. 2014,.
[23] Oomen T, Grassens E, Hendriks F, van Herpen R, Bosgra O. Inferential motion control: identification and robust control with unmeasured performance variables. In: Proceedings of the 50th IEEE Conference on Decision and Control and European Control Conference, Orlando, FL, USA. 2011, p. 964–9.
[24] Groot Wassink M, van de Wal M, Scherer C, Bosgra O. LPV control for a wafer stage: beyond the theoretical solution. Control Engineering Practice 2005;13(2):231–45.
[25] Oomen T, van de Wijdeven J, Bosgra O. Suppressing intersample behavior in iterative learning control. Automatica 2009;45(4):981–8.